Research Article

Synthesis of suitable material for microwave absorbing properties in X-band

Monika Rani[1] · Kamaljit Singh Bhatia[2] · Harjitpal Singh[3] · Harsimrat Kaur[3] · Nancy Gupta[4]

Received: 30 May 2020 / Accepted: 29 October 2020 / Published online: 20 November 2020

Abstract
Synthesization of M-type hexaferrite with composition $Ba_{0.5}Sr_{0.5}Co_xGa_xFe_{12-2x}O_{19}$ (x = 0.0, 0.2, 0.4, 0.6, 0.8, 1.0) has been performed at temperature 1100 °C for 15 h by adopting conventional ceramic method. For analyzing the structure of synthesized material, the X-ray diffraction (XRD) method has been used. Besides that its properties are observed by using different characterization techniques like VSM (vibrating sample magnetometer), Fourier Transform Infrared (FTIR) spectra and VNA (Vector network analyzer), SEM (scanning Electron Microscopy), Energy-dispersive X-ray spectroscopy (EDAX). Microwave absorption property has been investigated using quarter wavelength and impedance matching mechanism in the X-Band range (8.2–12.4 GHz). From the results obtained, it was being observed that microwave absorption was best at doping concentration x = 0.4 i.e. −33.36 dB reflection loss at thickness 2.0 mm and frequency 9.62 GHz. The synthesized samples can be used for different possible applications in X-Band as narrowband & broadband absorbers and EMI shielding devices. The main applications are Electromagnetic Compatibility, microwave filters, network switches, Radar cross-section reduction (RCS) in the military, electronic enclosures and antenna applications.

Keywords Microwave absorption · Doping · Reflection loss · Electromagnetic interference

1 Introduction

As today is the era of wireless communication and human being becomes very much dependent on various wireless communication technology like Wi-Fi, Wimax, mobile communication, LAN/WAN/MAN in their daily life. These huge electromagnetic signals in the atmosphere get intermixed and produce undesired signals in electrical and electronic devices. This is known as EMI (Electromagnetic interference). This prevention of EMI has attracted a lot of researchers to explore the materials that can absorb EMI or suppress EMI. Further, it has been found that M-type hexagonal ferrites have varying favorable properties in the GHz frequency range that make it a good microwave absorber. M-type ferrites have high structural and chemical stability, high electrical resistance, low density and low cost that make it the best choice among other classes of ferrites [1–3]. A lot of research work has been carried out in this field. Some researchers have investigated the magnetic and dielectric properties of doped and undoped ferrites while others have researched the absorption properties of ferrites [4, 5]. Khandani et al. formed a Ce-Nd doped Sr hexagonal ferrite that has given absorption properties in the X-band range. The observed RL was −8.7 dB at 2.5 mm thickness [6]. Singh et al. experimented to find the effect of doping on microwave absorption. He had used Mn^{2+} & Ti^{4+} as the dopant in M-type Sr hexaferrite and found that RL increased up to −14.68 dB at 12 GHz [7]. Afghahi et al.

✉ Harsimrat Kaur, simrat6@yahoo.com; er.harsimrat@gmail.com; Monika Rani, tutejamonika6@gmail.com; Kamaljit Singh Bhatia, kamalbhatia.er@gmail.com; Harjitpal Singh, harjit_nit@yahoo.co.in; Nancy Gupta, nancy.gupta24@gmail.com | [1]Department of Research and Development, Research Scholar IKGPTU, Jalandhar, India. [2]Department of ECE, G.B. Pant Institute of Engineering & Technology, Pauri Garhwal, Uttarakhand 246194, India. [3]Department of ECE, CTIEMT Shahpur, Jalandhar, Punjab, India. [4]Department of ECE, Lyallpur Khalsa College of Engineering, Jalandhar, India.

synthesized M–type $BaMg_xZn_xX_{2x}Fe_{12-4x}O_{19}$(X = Zr, Ce, Sn) & investigate reflection loss of −19.3 dB at 12.3 GHz [8]. Mosleh et al. formed M-type $Ba_{1-x}Ce_xFe_{12}O_{19}$ hexagonal ferrite that showed −16.43 dB reflection loss in X-Band [9]. Moradi et al. synthesized M-type hexagonal ferrite with composition $BaMg_{x/2}Mn_{x/2}Co_xTi_{2x}Fe_{12-4x}O_{19}$ wth RL of −17 dB in x = 0.5 at 10 GHz with thickness 2.7 mm [10]. Seifert et al. investigated the phase formation and magnetic properties of $Sr_{1-x}Ln_xFe_{12}O_{19}$ (Ln = Pr, Nd, Sm, Eu & Gd) hexaferrite [11] whereas K.K. Mallick has explored the magnetic and structural properties of M type barium hexaferrite [12]. Kadhkodyan et al. found enhanced microwave absorption property with the addition of phosphorous doping. The maximum RL was less than −30 dB at 1 mm thickness in X-Band [13]. Abdollahi et al. doped Ba hexagonal ferrite with La^{3+} and Gd^{3+} and got maximum RL of −7.8 dB at 10.4 GHz with thickness 3 mm [14]. Further, Velhal et al. reported a maximum RL of −37.49 dB in the X & Ku band by synthesization of Ba-Sr hexaferrite via in-situ polymerization method [15]. Veisi et al. has reported a minimum RL of −15.2 dB at 11.1 GHz with the addition of Cu/Zr doped Ba-Sr hexaferrite [16]. Later, Almessierea et al. had found Tb^{3+} doped hexaferrite as the best microwave absorber with RL −42.3 dB at 6.3 GHz and −11 dB & −15 dB around 15 GHz [17]. Septiani et al. had prepared Co-Ti doped Sr hexaferrite and observed −31 dB RL at frequency 7–13 GHz [18]. Later Khandani et al. had also done a synthesis of Ce-Nd doped Sr hexaferrite and observed −37 dB RL at 9.62 GHz at 2.5 mm thickness [19]. A comparison is done between the microwave absorption property of Ba hexaferrite with and without doping by Scozeri et al. [20] and found maximum RL of −41 dB with Cr^{3+} doping and −33 dB RL without doping in X-band.

S.P. Gairola et al. reported the magnetic and electromagnetic wave absorbing properties of the Co–Mn–Ti substituted barium ferrites, $BaCo_xMn_xTi_{2x}Fe_{12-4x}O_4$ ($0 \le x \ge 0.5$) and the maximum reflection loss (−14.7 dB) is observed for the x = 0.4 sample [21]. A.Ghasemi et al. synthesize M-type barium hexaferrite $BaFe_{12-x}(Mn_{0.5}Cu_{0.5}Ti)_{x/2}O_{19}$, with reflection loss more than −25 dB for specific frequencies [22]. Sukhleen Bindra Narang et al. characterize Co–Ti substituted ferrites with the general formula, $BaFe_{(12-2x)}Co_xTi_xO_{19}$ where $x = 0.0, 0.3, 0.5, 0.7$ and 0.9, the maximum absorption of 99% was obtained for the composition $x = 0.7$ with a peak value of reflection loss of −25.15 dB at a thickness of 3.3 mm [23]. To decide substitution agents, the crystal structure of ferrite has been deeply analyzed, as there are tetrahedral and octahedral sites present in different ferrite. The selection of Co and Ga is attributed to their large ionic radii and it can cause their occupancy on the octahedral site which makes them a soft ferrite nature required for the absorber. The X Band (8–12 GHz) has a short wavelength that allows for higher resolution imaging for target identification and discrimination and mainly used for radar applications. X-band is preferred because it has been assigned for deep space communications by the International Telecommunications Union (ITU).

We have already explored the results of synthesized M-type hexagonal ferrite with composition $Ba_{0.5}Sr_{0.5}Co_xGa_xFe_{12-2x}O_{19}$ (x = 0.0, 0.2, 0.4, 0.6, 0.8, 1.0) by ceramic method at temperature 1150 °C [24]. In this paper we have improved the results by varying the temperature conditions to 1100 °C and microwave absorption property has been evaluated using impedance matching and Quarter wavelength mechanism.

2 Experimental procedure

2.1 Preparation of hexagonal ferrite

Synthesization of $Ba_{0.5}Sr_{0.5}Co_xGa_xFe_{12-2x}O_{19}$ (x = 0.0, 0.2, 0.4, 0.6, 0.8, 1.0) has been done using conventional ceramic method. Materials used for the aforesaid experiment were $BaCo_3$ (AR grade Sigma Aldrich, 99.98% pure), $SrCo_3$ (AR grade Sigma Aldrich, 99.98% pure), $CoCo_3$ (AR grade Sigma Aldrich, 99.98% pure), Ga_2O_3 (AR grade Sigma Aldrich, 99.98% pure) & Fe_2O_3 (AR grade Sigma Aldrich, 99.98% pure). The stoichiometric amount of different chemical reagents of the compositions was ground using electrically controlled agate pestle and mortar in the presence of distilled water for 8 h. After drying the powder at room temperature, it was pre-sintered at 1000 °C for 10 h in an automatic electrical furnace which was programmed to do the same. Again, this powder was cooled down & reground for 8 h. In the last step, this fine powder was turned into a disk shape pallet using a hydraulic press at 75 KN/m^2 pressure. Then sintering of the pallet was done at 1100 °C for 15 h & slowly cooled down at room temperature to obtain hexagonal powder samples.

For the analysis of this synthesized material, we used different methods i.e XRD (X-ray diffraction method) for analysis of crystal structure, chemical bonding of material was analyzed using FTIR (Fourier transform infrared spectroscopy), VSM (vibrating sample magnetometer) for exploring the hysteresis properties, SEM (scanning Electron Microscopy) to study grain morphology and EDAX (Energy-dispersive X-ray spectroscopy) to confine chemical composition.

With the XRD method crystal structure is analyzed using the following equation:

$$\frac{1}{d_{hkl}^2} = \frac{4}{3}\left(\frac{h^2}{a^2} + \frac{hk}{a^2} + \frac{k^2}{a^2}\right) + \frac{l^2}{c^2} \quad (1)$$

where h, k, l are miller indices, d_{hkl} is the d-spacing of lines occurring in XRD pattern. Lattice constant a, c was found from the equation.

The size of the cell was determined using the equation:

$$D_{xrd} = \frac{0.9\lambda}{\beta_{1/2}\cos\theta} \quad (2)$$

This is a Debye Scherrer equation [14]. Where λ is 1.54056 Å is X-ray wavelength, β is the full width of major diffraction peaks, θ is Bragg angle.

Unit cell volume was calculated using equation [15]:

$$V_{cell} = \frac{\sqrt{3}}{2}a^2c \quad (3)$$

Based on the Archimedes principle, bulk density was calculated I.e.

$$\rho_x = \frac{2M}{N_A V_{cell}} \quad (4)$$

where M is molar mass, N_A is Avogadro's number. Its value is 6.0123×10^{23}/mole.

$$\text{Porosity } P = \left(1 + \frac{Dx}{Dm}\right) \times 100\% \quad (5)$$

where *Dx* is X-ray density and *Dm* bulk mass density.

Now the main part of research i.e. microwave absorption was being carried out using VNA (Vector network analyzer) method at X-band (8.2 GHz–12.4 GHz). But before using VNA for measurements, it is calibrated by doing measurements in air. For finding out absorption properties, complex permeability and complex permittivity were being measured.

Complex Permeability, $\mu_r = \mu' - j\mu''$, Complex Permittivity, $\varepsilon_r = \varepsilon' - j\varepsilon''$, where μ' is permeability, μ'' is magnetic loss, ε' is dielectric constant, ε'' is the dielectric loss.

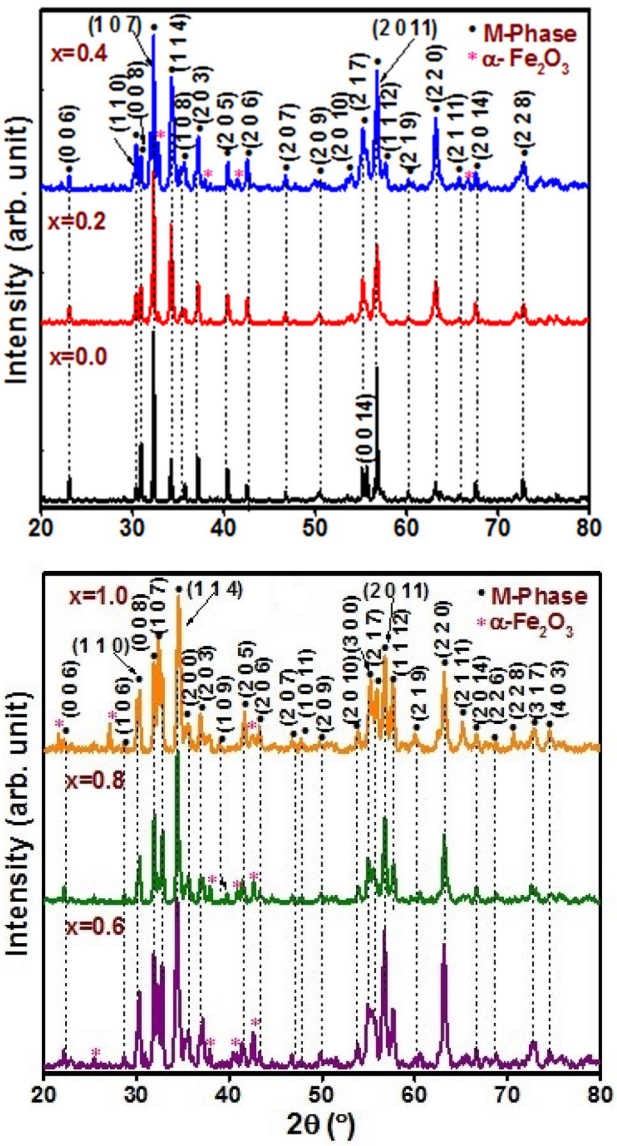

Fig. 1 (**a**) and (**b**) XRD (X-ray diffraction method) analysis of $Ba_{0.5}Sr_{0.5}Co_xGa_xFe_{12-2x}O_{19}$ (x = 0.0, 0.2, 0.4, 0.6, 0.8, 1.0) samples

3 Analysis of results

3.1 XRD analysis

During the analysis of the prepared hexagonal ferrite samples of $Ba_{0.5}Sr_{0.5}Co_xGa_xFe_{12-2x}O_{19}$ (x = 0.0, 0.2, 0.4, 0.6, 0.8, 1.0), we observed that for the composition x=0.0 & 0.2, there is only the primary phase of material but for x > 0.2, we observed another secondary phase of orthorhombic $BaFe_2O_4$.

The samples used are analyzed for their purity of the phase and other properties like how they respond to the applied force i.e. mechanical, using a diffraction technique which includes X-rays as the testing wave shown in Fig. 1a and b. The diffraction patterns formed through this analysis are calculated using Millar indices. The result shows that there is the formation of the hexagonal shaped M-type phase other than that no peak was observed in other phases. These peaks formed correspond to the M-type crystal structure formed in the JCPDS file no. 51-1879, a = 5.8862 Å, c = 23.137 Å and V = 694.24 $Å^3$.

The factors used in Table 1 have proximity to the pure compounds when faced with the X-ray waves. The composition formed in the space by the material is P63/mmc. The decrease in the cell volume and the lattice parameters shows the solubility due to smaller ionic radii of Ga^{3+}(0.62 Å) and Co^{2+} (0.72 Å) in M-Type hexaferrite lattice [15, 16]. Also, the X-ray density increased by 0.37 g/

Table 1 Lattice and hysteresis parameters of M-type $Ba_{0.5}Sr_{0.5}Co_xGa_xFe_{12-2x}O_{19}$ hexaferrites

x	a (Å)	c (Å)	c/a	Cell volume (Å^3)	Density		Porosity (%)	H_c (Oe)	H_a (kOe)	M_s (emu/g)	M_s/H_a (emu g^{-1}/KOe)	M_r (emu/g)	M_r/M_s
					XRD (g/cm^3)	Bulk (g/cm^3)							
0.0	5.871	23.077	3.930	688.84	5.20	3.98	23.35	260	9.35	56.2	6.01	7.4	0.13
0.2	5.866	23.075	3.933	687.61	5.22	3.74	28.33	845	9.28	60.0	6.46	6.8	0.11
0.4	5.862	23.089	3.938	687.09	5.24	4.38	16.39	155	6.83	49.1	7.18	5.8	0.11
0.6	5.819	23.059	3.962	676.16	5.34	4.19	21.61	195	6.71	62.0	9.23	8.0	0.12
0.8	5.812	23.015	3.959	673.25	5.38	4.10	23.75	95	4.76	54.0	11.34	4.8	0.08
1.0	5.795	23.004	3.969	669.00	5.43	3.85	29.20	75	4.45	56.5	12.69	4.1	0.07

cm^3 as it is directly proportional to the molecular weight using Eq. (2), this is all compared to the Fe^{3+} ionic radii and molecular weight (0.64 Å, 55.84 amu). The doping also affects the crystalize size as it decreases in comparison to the undoped ones. The c/a ratio is used to measure the type of the structure of the composition and here the ratio comes out to be in the range of 3.93–3.96 which is lower than of 3.98 to conclude magneto plumbite type structure [18].

Table 1 can be used to calculate the hysteresis parameters, which are compared in Fig. 2. The saturation law is used for the calculation of the anisotropy field (H_a) and saturation magnetization.

For designing the microwave absorbers, a small value of coercivity is desired and which is achieved by doping. Coercivity depends on the intrinsic (anisotropy field) and extrinsic (grain size) factors. It changes, inversely with grain size and directly with the porosity. Doping shows non-linear variations in the size of the grain and porosity. With the doping the anisotropy field varies linearly, it is highest 9.35 kOe in x = 0.0 and lowest 4.45 kOe in x = 1.0. The porosity variation affects the anisotropy field in nonlinear passion. There is the highest porosity with the minimum field for composition x = 1.0; this introduces the factor; site occupancy which affects the field [20]. The site occupancy of the $Co^{2+}$and Ga^{3+} is 4f2 and 2b. There is a non-linear variation in the value of H_a and H_c due to extrinsic and intrinsic factors with the doping.

Similarly, magnetic saturation does not only depend upon porosity but also on site occupancy of spin up and spin down sites by Co^{2+} and Fe^{3+}. M_s decreases with occupancy of ions on spin up sites (12k, 2a, and 2b) and M_s increases with occupancy of ions on spin down sites ($4f_1$ and $4f_2$) [21]. M_s has maximum value of 62.0 emu/g in x = 0.6 and minimum value as 49.1 emu/g for composition x = 0.4. M_s increases from x = 0.0 to x = 0.2 due occupancy of ions on spin down sites ($4f_1$ and $4f_2$) and from x = 0.6 to x = 1.0 decreases with occupancy of ions on spin up sites (12k, 2a, and 2b).

3.2 FTIR analysis

For the prepared samples ferrite formation confirmation was also done by using Fourier transform infrared (FTIR) spectra (Fig. 3) which are available in the wavenumber range from 300 to 600 cm^{-1}. Two main dips in the spectra represent the v1-mode (near to 520 cm^{-1}) and v2 (near to 300–600 cm$^{-1)}$ modes respectively. These two modes are per the tetrahedral and octahedral sites of M-type hexagonal ferrite. The metal oxide (Fe^{3+}–O^{2-}) stretching vibrations

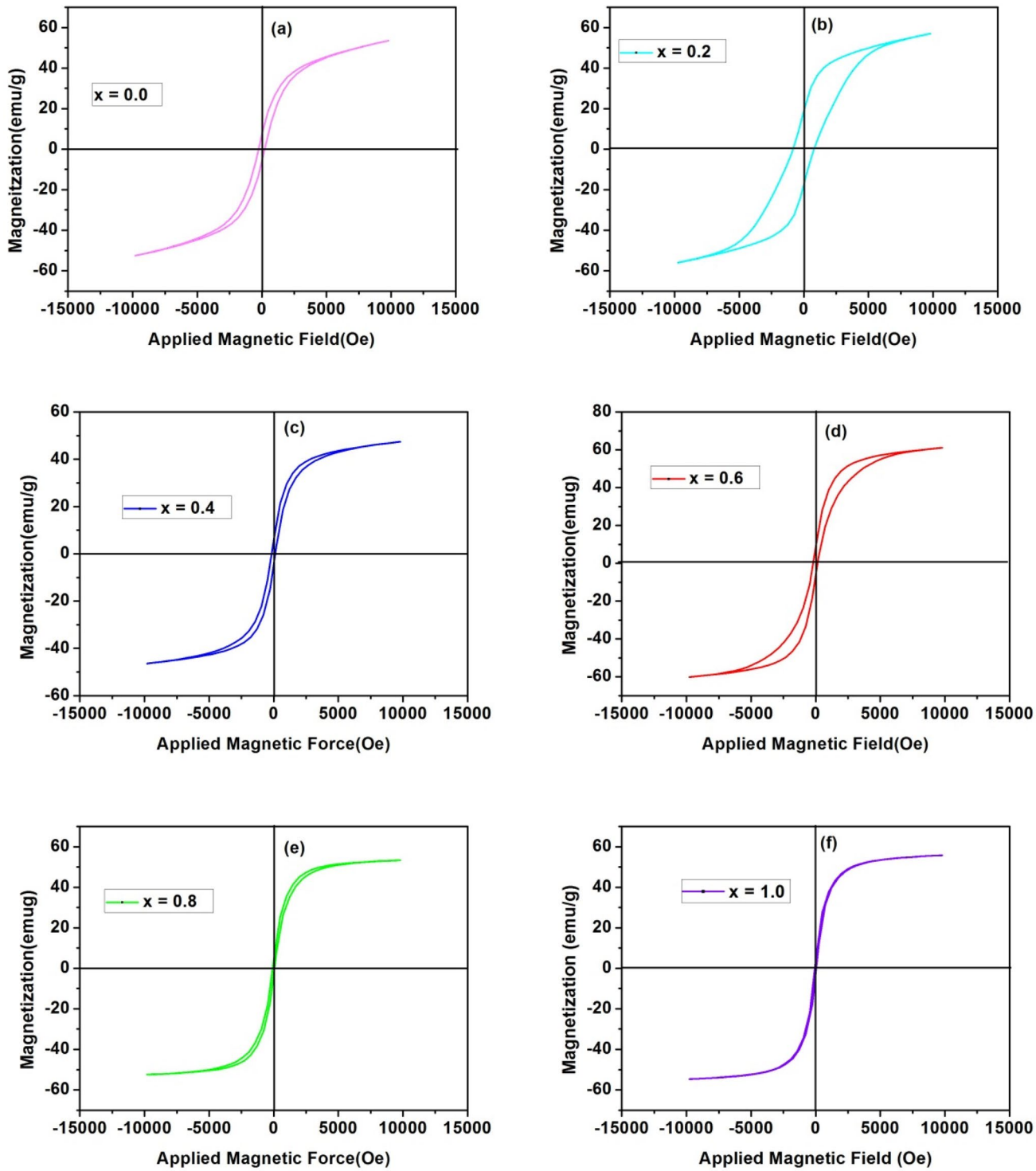

Fig. 2 VSM (vibrating sample magnetometer) for exploring the hysteresis properties of $Ba_{0.5}Sr_{0.5}Co_xGa_xFe_{12-2x}O_{19}$ (x = 0.0, 0.2, 0.4, 0.6, 0.8, 1.0) samples

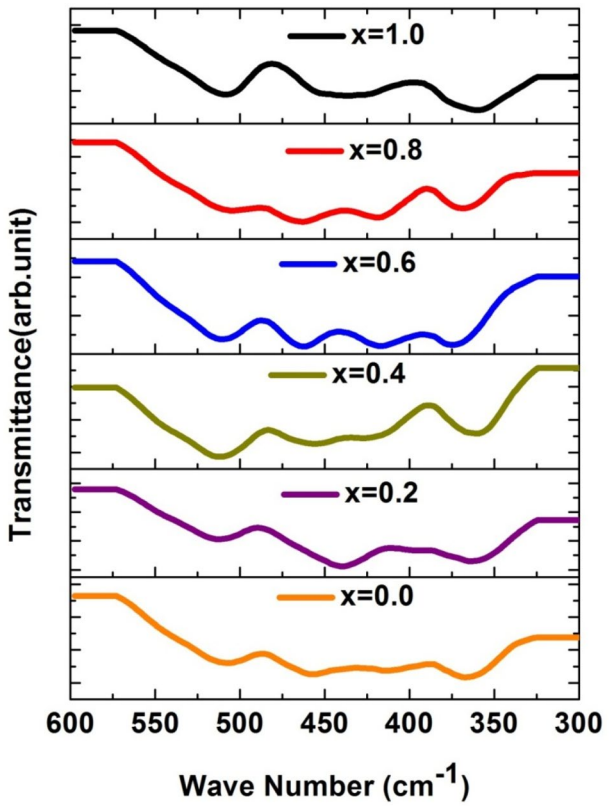

Fig. 3 Fourier Transform Infrared (FTIR) spectra of M-type $Ba_{0.5}Sr_{0.5}Co_xGa_xFe_{12-2x}O_{19}$ hexagonal ferrite

are associated with these bands. The change in position of these bands may be due to the change in Fe^{3+}–O^{2-} the distance between tetrahedral and octahedral coordination. These results confirmed the ferrite formation [16, 17].

3.3 Scanned electron micrograph (SEM)

The scanned electron micrographs of the undoped (x = 0.0) and doped composition (x = 0.4, 0.6, 1.0) show that the grain size was larger before the doping and later its size decreases with doping. The grains in the doped composition exhibits non-uniformity in size and distribution. The non-uniformity after the doping results in the presence of the large and small grains at higher doping levels shown in Fig. 4. Despite large ionic radii of substituted Co^{2+}–Ga^{3+} cations than Fe^{3+} ions, the grain size of the cluster was found to decrease with substitution. So, substitution inhibited grain growth.

3.4 Energy dispersive spectra (EDAX)

To confirm the chemical composition of $Ba_{0.5}Sr_{0.5}Co_xGa_xFe_{12-2x}O_{19}$ hexagonal ferrites synthesized using a standard ceramic method and sintered at 1100 °C for 15 h, the energy dispersive spectra (EDAX) of the typical compositions (x = 0.2, 0.4, 0.6, 0.8 and 1.0) were recorded at room temperature and obtained EDAX spectra are shown in Fig. 5. The EDAX spectra of all samples explain the presence of Ba, Sr, Fe, Co and Ga in all compositions.

The observed chemical composition data of the same compositions are summarized in Table 2. It is observed that some other extra element is also observed in the compositions of 0.4 and 0.6. The weight ratio and atomic weight ratios as observed from EDAX are also mentioned in Table 2.

3.5 Complex permittivity and permeability

With the addition of dopant elements in hexagonal ferrite, complex permittivity ($\varepsilon' - j\varepsilon''$) and complex permeability ($\mu' - j\mu''$) varies non linearly with frequency 8.2 GHz–12.4 GHz. With the increase in frequency, the dielectric constant decreases. This behavior could be explained by Koop's phenomenological theory. The dielectric loss (tan δ_ε) and magnetic loss (tan $\delta_{\mu)}$ represent the dissipation of energy. It is determined by the following relation:

$$\tan \delta_\varepsilon = \varepsilon''/\varepsilon' \quad (6)$$

Similarly,

$$\tan \delta_\mu = \mu''/\mu' \quad (7)$$

where ε″, ε′, μ″, μ′ represent dielectric loss, dielectric constant, magnetic loss and permeability. The loss tangent decreases with an increase in frequency. This is due to the hopping frequency of electrons, which can't follow the variation in the polarity of the external field after a certain frequency. In Fig. 6 the value of dielectric constant (ε′) is lowest in x = 1.0 composition highest with x = 0.2. With the rest of the compositions, ε′ is varying non linearly. Whereas dielectric losses(ε'') are maximum at x = 0.4. According to Maxwell–Wagner theory, both ε′ and tan δ_ε are inversely proportional with frequency. The more value of tan δ_μ in comparison of tan δ_ε shows that tan δ_μ contributes more to absorption as compared to tan δ_ε.

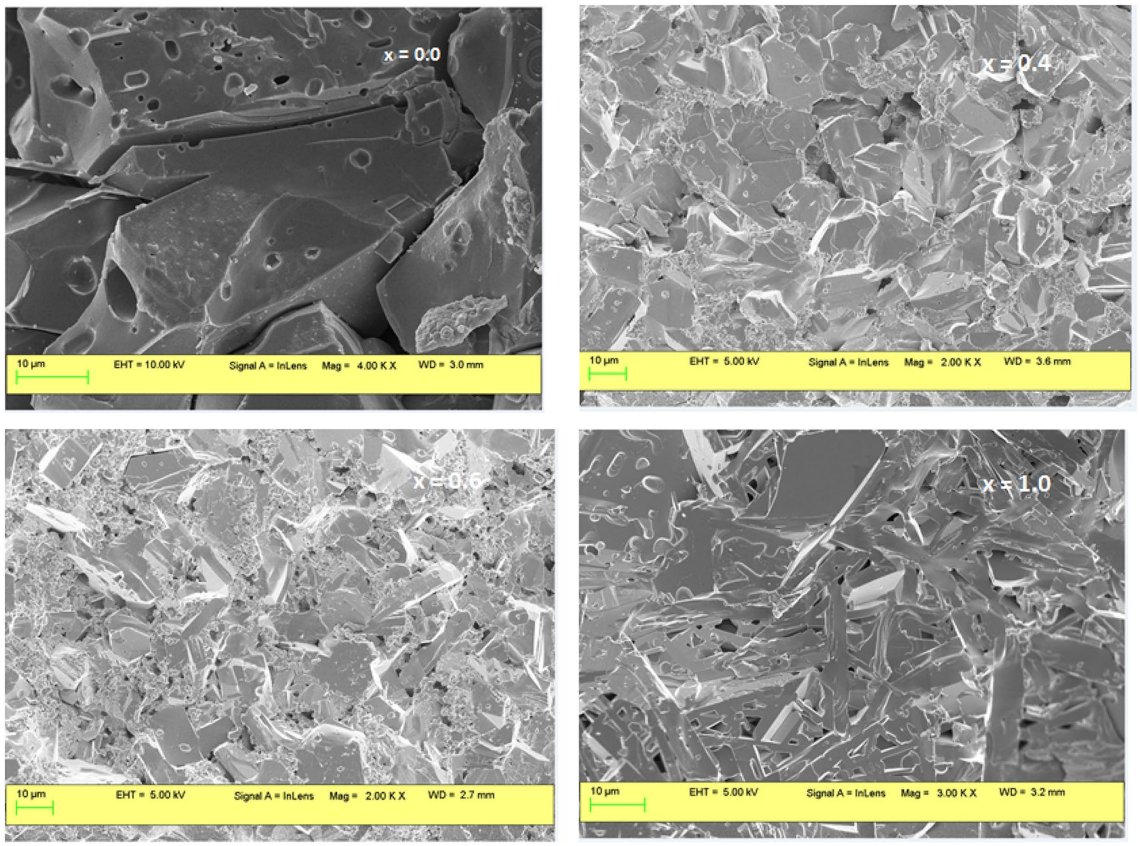

Fig. 4 Scanned electron micrographs of $Ba_{0.5}Sr_{0.5}Co_xGa_xFe_{12-2x}O_{19}$ (x = 0.0, 0.4, 0.6 and 1.0) hexagonal ferrite compositions

3.6 Microwave absorption and reflection loss analysis

For the synthesized ferrites to be a good absorber, its reflection loss value should be below −10 dB. As we have prepared the samples for not only different compositions i.e. varying from x = 0.0, 0.2, 0.4, 0.6, 0.8 and 1.0 but also at varying thicknesses too. We have plotted the graph between frequency and reflection losses for synthesized material of varying doping with different thicknesses as shown in Fig. 7. It is observed that there is a large variation in RL peaks with a doping concentration of Co^{2+} and Ga^{3+}. All doping concentrations have reflection loss less than −10 dB and x = 0.4 is best among all as it has large absorption (RL is −33.36) for the thickness of 2.0 and at frequency 9.62 GHz. The reflection loss dips are affected by frequency, doping and thickness of composition. A single peak represents a single frequency band for microwave absorption whereas two reflection peaks indicate that it has maximum absorption in two bands.

3.7 Analysis of results with quarter-wavelength mechanism

According to the quarter wavelength mechanism, a material having thickness equal to λ/4 of the wavelength of microwave signal will have maximum absorption [17, 18]. Whenever a ferrite material having a metal plate at the far end is placed in a waveguide & microwave signal is fed, a certain portion of the signal will be reflected and the rest get transmitted through ferrite. But this rest of the portion again gets reflected by the metal end towards the front surface. When both the signals are 180° out of phase, they get canceled and the total reflection is zero.

Mathematically, it is given by the following equation:

$$t_m = \frac{n\lambda_0}{4\sqrt{\mu\varepsilon}} \quad \text{where } n = 1, 3, 5 \ldots \tag{8}$$

Here t_m is the thickness of the material, λ_o free-space wavelength, ε is complex permittivity, μ is complex

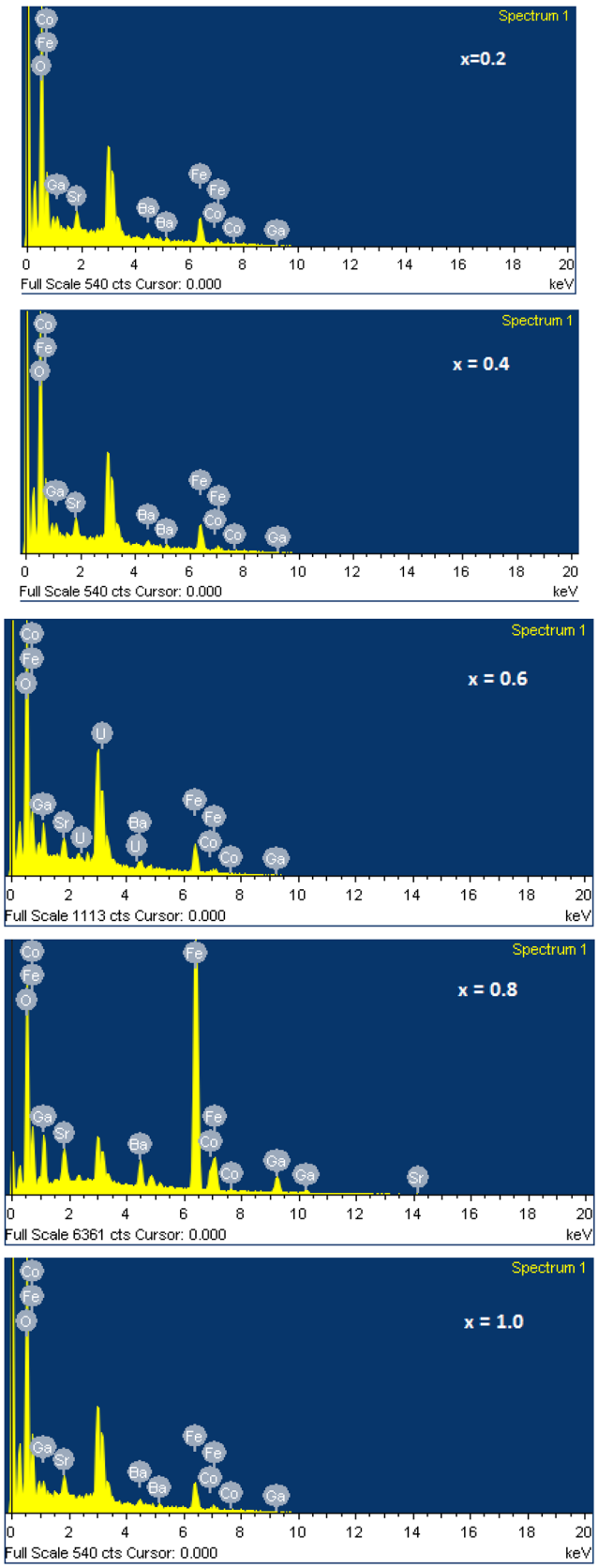

Fig. 5 Energy dispersive spectroscopy spectra of $Ba_{0.5}Sr_{0.5}Co_xGa_xFe_{12-2x}O_{19}$ (x = 0.2, 0.4, 0.6, 0.8 and 1.0) hexagonal ferrite compositions

permeability. Values of complex permittivity (ε) and complex permeability (μ) are calculated by using the Nicholson-Ross-Weir (NRW) method which provides a direct calculation of both the permittivity and permeability from the s-parameters. It is the most commonly used method for performing such conversion. Measurement of reflection coefficient and transmission coefficient requires all four (S11, S21, S12, S22) or a pair (S11, S21) of s-parameters of the material under test to be measured. It is clear from the results shown in Table 3 and Fig. 8 that there is a negligible difference in the measured and calculated thickness of material for all compositions so we can say that the process obeys the quarter wavelength mechanism. Besides that, we can observe that for composition x = 0.4, we also get maximum RL as −33.36 dB at frequency 9.62 with a thickness as 2.0.

Table 4 depicts the absorption bandwidth (ABW) for samples of all compositions at different thicknesses with their corresponding RL peaks for in-between −10 dB to −20 dB and more than −20 dB. Depending on available applications in X-Band i.e. 8.2–12.4 GHz, we can use these compositions as narrowband and wideband absorbers. While describing microwave absorber, bandwidth is also considered as another important parameter. Table 4 explains that at composition x = 0.8 it can act as wideband absorber (B.W = 4.2GHz) with thickness t = 2.0 mm & as a narrowband absorber (B.W = 0.17 GHz) at thickness t = 1.5 mm, with reflection loss varying from −10 dB to −20 dB and similarly it operates in wideband for composition x = 0.4 (B.W = 1.1 GHz) with thickness of 2 mm & as narrowband (B.W = 0.08 GHz) for composition x = 1.0 with reflection loss varying from −10 dB to −20 dB for t = 3.0 mm. Figure 9 displays 10-dB and 20-dB bandwidth for the RL peaks of different compositions. It can be seen that 10-dB and −20-dB bandwidth is minimum in composition x = 0.0 and a maximum value of 4.2 GHz occurs in substituted composition x = 0.8, covering the whole X-band spectrum.

3.8 Analysis of impedance matching mechanism

This impedance matching mechanism states that microwave absorption of the signal will be maximum when $Z_{in} = Z_o$ i.e. input impedance is the same as characteristic impedance. This is the criterion of transmission line theory [21]. According to this:

$$Z_{in} = Z_o \sqrt{\frac{\mu_r}{\varepsilon_r}} \tanh\left[j\left(\frac{2\pi ft}{c}\right)\left(\sqrt{\mu_r \varepsilon_r}\right)\right] \quad (9)$$

Table 2 Elemental composition weight & atomic percentage of typical samples of $Ba_{0.5}Sr_{0.5}Co_xGa_xFe_{12-2x}O_{19}$ (x = 0.2, 0.4, 0.6, 0.8 and 1.0) hexagonal ferrites

Element	Weight (%)	Atomic (%)	Weight (%)	Atomic (%)	Weight (%)	Atomic (%)	Weight (%)	Atomic (%)	Weight (%)	Atomic (%)
	0.2		0.4		0.6		0.8		1.0	
O	30.92	64.71	22.94	62.54	23.46	63.12	25.06	56.54	30.92	64.71
Fe	49.37	29.60	28.74	22.45	24.82	19.14	49.98	32.24	49.37	29.60
Co	− 1.78	− 1.01	5.14	3.80	7.72	5.64	4.12	2.52	−1.78	−1.01
Ga	3.35	1.61	2.71	1.70	4.68	2.89	10.15	5.25	3.35	1.61
Sr	4.84	1.85	3.48	1.73	3.45	1.69	4.05	1.67	4.84	1.85
Ba	13.31	3.24	7.45	2.37	7.73	2.42	6.75	1.77	13.31	3.24
U			29.54	5.41	28.15	5.09				
Total	100%		100%		100%		100%		100%	

Here $Z_o = 377\ \Omega$ for free space, ε_r is complex permittivity, μ_r is complex permeability, t is the thickness of the material, f is the frequency and c is the velocity of light.

As $Z_{in} = a + jb$. Where 'a' is the real part of impedance i.e. Z_{real} & b is the imaginary part of impedance i.e Z_{img}. If $Z_{real} = 377\ \Omega$ & $Z_{img} = 0$ then the whole signal gets absorbed but in actual it is not so. That's why microwave absorption decreases as shown in the graph plotted between impedance and frequency as shown in Fig. 10. It is clear from the graph that x = 0.2, 0.4, 0.8 have Z_{real} & Z_{img} closed to 377 Ω & 0 than x = 0.0, 0.6 & 1.0. So, x = 0.2, 0.4, 0.8 gave better microwave absorption comparatively.

Table 5 gives the values of Z_{real} and Z_{imag} for all compositions at their respective RL peaks and corresponding frequencies. For the composition x = 0.4, we observed a maximum RL peak of −33 dB at frequency 9.62 GHz and Z_{real} as 362.49 Ω closest to 377 Ω & Z_{img} as −6.44, which is close to zero. So, we can conclude that the process fully satisfies the impedance mechanism too.

In Fig. 11 the reflectivity with frequency has been plotted for x = 0.4 with a thickness of 0.2 mm. The result shows that the maximum absorption occurs at 9.6 GHz which is in agreement with the minimum reflection of an incident wave from the material at the same frequency of 9.6 GHz. The reflectivity of the normal incident electromagnetic wave can be calculated from the following formula:

$$\text{Reflectivity } R = \frac{1 - Z}{1 + Z} \tag{10}$$

where $Z = \sqrt{\mu/\varepsilon}$.

4 Conclusion

We have successfully synthesized and analyzed Ba-Sr hexagonal ferrite with composition $Ba_{0.5}Sr_{0.5}Co_xGa_xFe_{12-2x}O_{19}$ (x = 0.0, 0.2, 0.4, 0.6, 0.8. 1.0) using standard ceramic method and confirmed hexagonal structure using XRD analysis. The samples also show perfect magnetic properties as a result of the maximum M_s value of 62.0 emu/g in x = 0.6 and minimum value as 49.1 emu/g for composition x = 0.4. The observed characteristic absorption bands, v1-mode around 520 cm^{-1} and v2-mode around 360, 370 cm^{-1}, are related to the tetrahedral and octahedral sites respectively of M-type hexagonal ferrite. All doping concentrations have minimum absorbed power and x = 0.4 is best among all as it has large absorption (RL is −33.36) for the thickness of 2.0 mm and at frequency 9.62 GHz. The process completely satisfies the quarter wavelength mechanism and impedance mechanism criterion. The material synthesized owes good scope for wideband and narrowband absorber applications and used to suppress EMI in the application such as radar, satellite, mobile phones, WiFi, Wi-Max, etc.

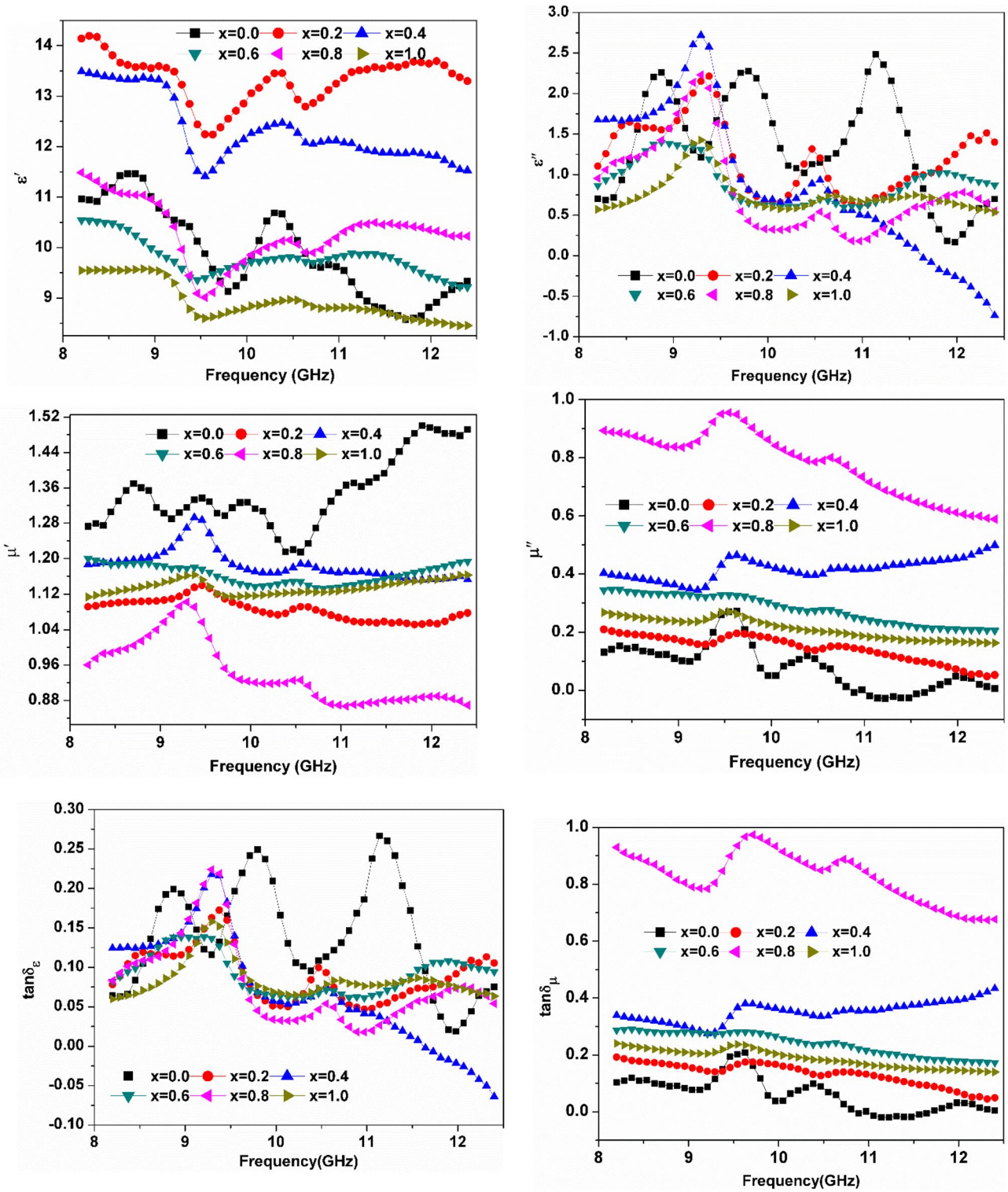

Fig. 6 Variation of ε′, ε″, μ′, μ″, $\tan\delta_\varepsilon$ and $\tan\delta_\mu$ as a function of frequency in M-type $Ba_{0.5}Sr_{0.5}Co_xGa_xFe_{12-2x}O_{19}$ hexagonal ferrite

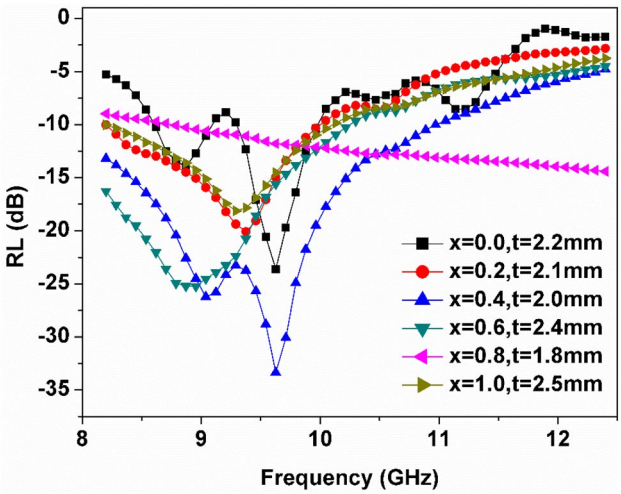

Fig. 7 Variations of RL peaks w.r.t frequency of $Ba_{0.5}Sr_{0.5}Co_xGa_xFe_{12-2x}O_{19}$ (x = 0.0, 0.2, 0.4, 0.6, 0.8, and 1.0) samples

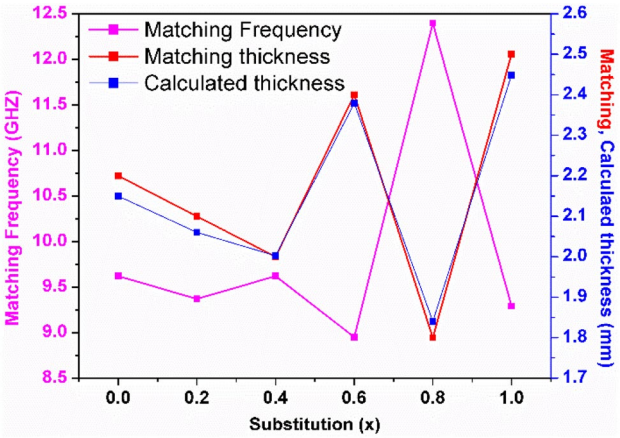

Fig. 8 Variation of measured thickness and calculated thickness with frequency and substitution in $Ba_{0.5}Sr_{0.5}Co_xGa_xFe_{12-2x}O_{19}$ (x = 0.0, 0.2, 0.4, 0.6, 0.8 and 1.0) samples

Table 3 Matching frequency, measured thickness and calculated thickness in $Ba_{0.5}Sr_{0.5}Co_xGa_xFe_{12-2x}O_{19}$ (x = 0.0, 0.2, 0.4, 0.6, 0.8 and 1.0) samples

Co-Ga doping	Matching frequency (f_{mat}) (GHz)	Matching thickness (mm) (measured)	Thickness t = nλ/4 (mm) (calculated) quarter wavelength mechanism
0.0	9.62	2.2	2.15
0.2	9.37	2.1	2.06
0.4	9.62	2.0	2.002
0.6	8.95	2.4	2.379
0.8	12.4	1.8	1.84
1.0	9.29	2.5	2.449

Table 4 Matching thickness, matching frequency, frequency band and absorption bandwidth for RL > −10 dB and −20 dB in M-type $Ba_{0.5}Sr_{0.5}Co_xGa_xFe_{12-2x}O_{19}$ hexaferrites

x	Max. RL (dB)	Matching thickness (mm)	Matching frequency (GHz)	Frequency band RL > −10 dB (GHz)	−10 dB absorption bandwidth (GHz)	Frequency band RL > −20 dB (GHz)	−20 dB absorption bandwidth (GHz)
0.0	−13.53	2.0	9.54	9.46–9.79		–	–
	−17.84	2.1	9.54	9.37–9.88		–	–
	−23.68	2.2	9.62	8.62–9.04 & 9.71–9.96	0.42 & 0.25	9.54–9.62	0.08
	−20.84	2.3	9.62	8.62–9.04	0.42	9.62–9.71	0.09
	−16.50	2.4	9.71	8.70–9.04 & 9.46–9.88	0.34 & 0.42	–	–
	−13.17	2.5	9.71	9.54–9.88	0.34	–	–
	−10.86	2.6	9.71	9.62–9.79	0.28	–	–
0.2	−10.51	1.8	10.46	10.46–10.55	0.09		
	−12.45	1.9	10.46	10.04–10.72	0.68		
	−14.87	2.0	9.37	8.78–10.55	1.77		
	−20.08	2.1	9.37	8.2–9.96	1.76		
	−17.49	2.2	8.53	8.2–9.79	1.59		
	−18.37	2.3	8.45	8.2–9.62	1.42		
	−14.80	2.4	8.2	8.2–8.95	0.7		
	−11.41	2.5	8.2	8.2–8.53	0.33		
0.4	−18.28	1.5	12.4	10.97–12.4	1.43		
	−20.93	1.6	11.89	10.21–11.64	1.43	11.72–12.06	0.34
	−25.08	1.7	11.14	9.37–10.72 & 11.64–12.4	1.35 & 0.76	10.80–10.96	0.16
	−32.14	1.8	10.55	8.78–10.04 & 11.05–11.98	1.26 & 0.93	10.13–10.97	0.84
	−32 to 34	1.9	9.96	8.2–9.54 & 10.38–11.47	1.34 & 1.09	9.62–10.30	0.68
	−33.36	2.0	9.62	8.2–8.70 & 9.96–10.97	0.5 & 1.01	8.78–9.88	1.1
	−28.90	2.1	8.70	8.2–8.28 & 9.12–10.30	0.08 & 1.18	8.36–9.04	0.68
	−25.85	2.2	8.28	8.70–9.96	1.26	8.20–8.62	0.42
	−19.87	2.3	8.2	8.2–9.71	1.51		
	−14.65	2.4	8.2	8.2–8.78	0.58		
	−11.50	2.5	8.2	8.2–8.45	0.25		
0.6	−11.58	1.8	11.89	11.39–12.4	1.01		
	−13.11	1.9	11.72	10.46–12.4	1.94		
	−13.25	2.0	10.63	9.71–12.23	2.52		
	−14.55	2.1	10.63	8.62–11.72	3.1		
	−15.60	2.2	9.79	8.2–10.97	2.35		
	−20.31	2.3	9.28	8.2–9.12 & 9.37–10.72	0.92 & 1.35	9.20–9.29	0.09
	−25.22	2.4	8.95	8.2–8.45 & 9.46–10.21	0.25 & 0.75	8.53–9.37	0.84
	−20.94	2.5	8.36	8.87–9.96	1.76	8.28–8.78	0.5
	−17.73	2.6	8.2	8.2–9.62	1.42		
	−14.38	2.7	8.2	8.2–9.46	1.26		
	−11.69	2.8	8.2	8.2–8.95	0.75		

Table 4 (continued)

x	Max. RL (dB)	Matching thickness (mm)	Matching frequency (GHz)	Frequency band RL > −10 dB (GHz)	−10 dB absorption bandwidth (GHz)	Frequency band RL > −20 dB (GHz)	−20 dB absorption bandwidth (GHz)
0.8	−10.20	1.5	12.4	12.23–12.4	0.17		
	−12.26	1.6	12.4	10.46–12.4	1.94		
	−14.06	1.7	12.4	9.37–12.4	3.03		
	−14.41	1.8	12.4	8.78–12.4	3.62		
	−13.47	1.9	10.38	8.28–12.4	4.12		
	−13.51	2.0	9.96	8.2–12.4	4.2		
	−13.53	2.1	9.62	8.2–11.98	3.78		
	−13.05	2.2	9.54	8.2–10.97	2.77		
	−12.29	2.3	9.54	8.2–10.30	2.1		
	−11.39	2.4	9.54	8.2–9.88	1.68		
	−10.50	2.5	9.46	8.2–8.62	0.42		
1.0	−11.01	2.2	10.63	10.30–10.97	0.67		
	−13.03	2.3	9.29	8.95–10.80	1.85		
	−16.15	2.4	9.29	8.62–10.30	2.02		
	−18.12	2.5	9.29	8.28–10.04	1.76		
	−16.57	2.6	9.37	8.2–9.88	1.68		
	−13.92	2.7	9.37	8.2–9.71	1.51		
	−13.66	2.8	8.2	8.2–9.54	1.34		
	−12.63	2.9	8.2	8.2–8.62	0.42		
	−11.0	3.0	8.2	8.2–8.28	0.08		

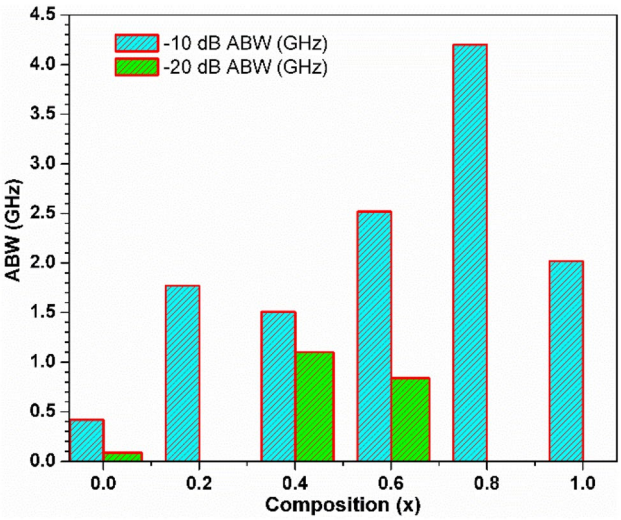

Fig. 9 Variation of maximum absorption bandwidth in compositions x = 0.0, 0.2, 0.4 ,0.6,0.8 and 1.0

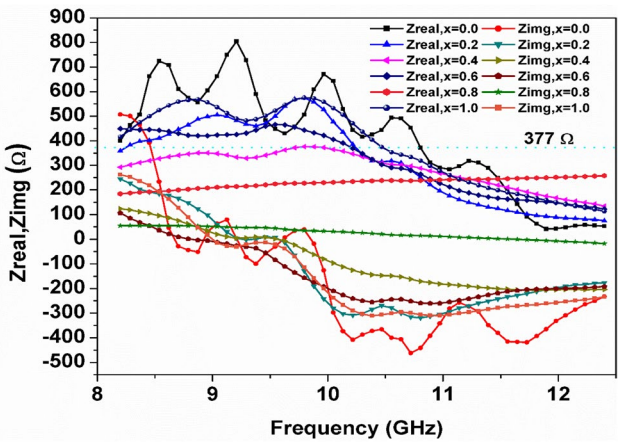

Fig. 10 Impedance matching mechanism with frequency, Z_{real} and Z_{img} values corresponding to the peaks in RL parameter in $Ba_{0.5}Sr_{0.5}Co_xGa_xFe_{12-2x}O_{19}$ (x = 0.0, 0.2, 0.4, 0.6, 0.8 and 1.0) samples

Table 5 Z_{real}, Z_{img} values of RL Peak at various thicknesses in $Ba_{0.5}Sr_{0.5}Co_xGa_xFe_{12-2x}O_{19}$ hexaferrite

Composition	Frequency (GHz)	RL (dB)	Z_{real} (Ω)	Z_{imag} (Ω)
x = 0.0	9.62	−23.68	429.12	7.89
x = 0.2	9.37	−20.08	459.87	1.14
x = 0.4	9.62	−33.36	362.49	−6.44
x = 0.6	8.95	−25.22	420.42	−4.98
x = 0.8	12.4	−14.41	257.55	−17.31
x = 1.0	9.29	−18.12	481.59	−20.57

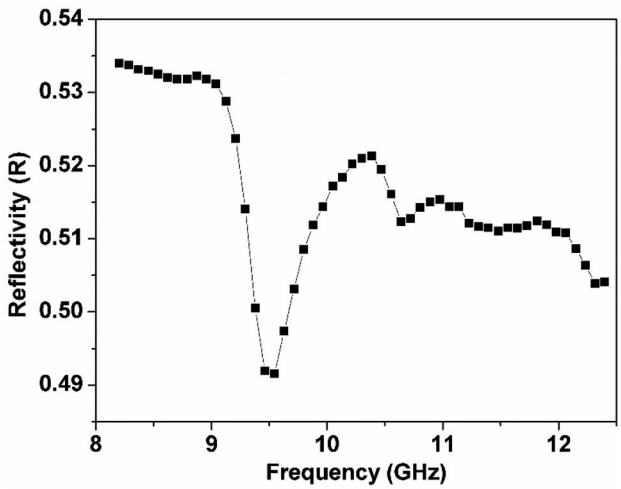

Fig. 11 Variation of reflectivity loss (R) of $Ba_{0.5}Sr_{0.5}Co_xGa_xFe_{12-2x}O_{19}$ with frequency

Compliance with ethical standards

Conflict of interest On behalf of all the co-authors, It is hereby to declare that in our submission of a research article entitled "Synthesis of suitable material for microwave absorbing properties in X-band" is an original work and there is no any conflict of interest for the same for any author.

References

1. Kim YJ, Kim SS (2002) Microwave absorbing properties of Co-substituted Ni/sub2/W hexaferrite in Ka-Band frequencies (26.5-40GHz). IEEE Trans Magn 38:3108–3110
2. Pullar RC (2012) Hexagonal ferrites: A review of the synthesis, properties and application of hexaferrite ceramics. Prog Mater Sci 57:1191–1334
3. Li ZW, Chen L, Ong CK (2002) Studies of static and high-frequency magnetic properties for M-type ferrite $BaFe_{12-2x}Co_xZr_xO_{19}$. J Appl Phys 92:3902–3907
4. Ravinder D, Reddy PVB (2003) High-frequency dielectric behavior of Li-Mg ferrites. Mater Lett 57:4344–4350
5. Liu X (2006) Research on La^{3+}-Co^{2+} substituted strontium ferrite magnets for high intrinsic coercive force. J Magn Mater 305(2):524–528
6. Khandani M, Yousefi M, Afghahi SSS, Amini MM, Bikhof Torbati M (2019) An investigation of structural and magnetic properties of Ce-Nd doped strontium hexaferrite nanoparticles as a microwave absorbent, mater. Chem Phys 235:121722–121738
7. Singh C, Kaur H, Bindra Narang S, Kaur P, Kaur R, Dhiman T (2016) Investigation of microwave absorption and DC electrical properties of Mn^{2+} and Ti^{4+} substituted $SrMn_xTi_xFe_{(12-2x)}O_{19}$ ferrite. J Alloys Compd 683:302–307
8. Afghahi SSS, Jafarian M, Atassi Y (2006) Microstructural and magnetic studies on $BaMg_xZn_xX_{2x}Fe_{12-4x}O_{19}$(x=Zr, Ce, Sn) prepared via mechanical activation method to act as a microwave absorber in X-Band. J Magn Mater 406:184–191
9. Mosleh Z, Kameli P, Poorbaferani A, Ranibar M, Salamati H (2016) Structural, magnetic and microwave absorption properties of Ce-doped barium hexaferrite. J Magn Magn Mater 397:101–107
10. Alam RS, Moradi M, Nikmanesh H, Ventura J, Rostami M (2016) Magnetic and Microwave absorption properties of $BaMg_{x/2}Mn_{x/2}Co_xTi_{2x}Fe_{12-4x}O_{19}$ hexaferrite nanoparticles. J Magn Magn Mater 402:20–27
11. Seifert D, Topfer J, Stadelbauer M, Grossinger R, Le Breton JM (2011) Rare-earth-substituted $Sr_{1-x}Ln_xFe_{12}O_{19}$ hexagonal ferrites. J Am Ceram Soc 94(7):2109–2118
12. Mallick KK (2007) Magnetic and structural properties of M-Type Ba hexaferrite prepared by co-precipitation. J Magn Magn Mater 311:683–692
13. Kadkhodyan H, Syed Dorraji MS, Rasoulifard MH, Amani-Ghadim AR, Hajimiri I, Tarighati Sareshk AR (2018) Enhanced microwave absorption property of $MnFe_{9n+3}O_{15n+4(0<n<1)}$ (M = Ba,Sr)/$CaCu_3Ti_4O_{12}$/phosphorus-doped g-C_3N_4 nanocomposite: Preparation and optimization. JALCOM 735:2497–2506
14. Abdollahi F, Yousefi M, Hekmati M, Khajehnezhad A, Salman S, Afghahi S (2019) Magnetic and Microwave Absorption Properties of Barium Hexaferrite Doped with La^{3+} and Gd^{3+}. J Nanostruct 9(3):579–586
15. Velhal N, Patil ND, Kulkarni G, Shinde SK, Valekar NJ, Barshilia HC, Puri V (2019) Electromagnetic shielding, magnetic and microwave absorbing properties of Polypyrrole/$Ba_{0.6}$ $Sr_{0.4}$ $Fe_{12}O_{19}$ composite synthesized via in-situ polymerization technique. JALCOM 777:627–637
16. Shooshtary Veisi S, Yousefi M, Amini MM, Shakeri AR, Bagherzadeh M (2019) Magnetic and microwave absorption properties of Cu/Zr doped M type Ba/Sr hexaferrite prepared via sol-gel auto-combustion method. JALCOM 773:1187–1194
17. Almessiere MA, Sozeri H, Trukhanov AV, Slimani Y, Ali S, Acar E, Baykal A (2019) Tb^{3+} ion substituted Sr hexaferrites as high quality microwave absorbers. JMMM 491:165595
18. Septiani A, Sanjaya HI, Dedi (2019) Magnetic and microwave absorbing properties of Co and Ti-doped Sr M-type hexaferrites in the X-band frequencies. In: International Conference on Radar, Antenna, Microwave, Electronics, and Telecommunications (ICRAMET), vol 4, pp 131–134. IEEE Catalog Number: CFP19C07-ART, ISBN: 978-1-7281-2482-7
19. Khandani M, Yousefi M, Afghahi SSS, Amini MM, Bikhof Torbati M (2019) An investigation of structural and magnetic properties of Ce-Nd doped strontium hexaferrite nanoparticles as a microwave absorbent. Mater Chem Phys 235:121722
20. Scozeri H, Genc F, Almessiere MA, Unver IS, Korkmaz AD (2019) Cr^{3+} substituted Ba Nano hexaferrites as high quality microwave absorber in X-band. JALCOM 779:420–426
21. Gairola SP, Verma V, Singha A, Purohit LP, Kotnala RK (2010) Modified composition of barium ferrite to act as a microwave absorber in X-band frequencies. Solid State Commun 150(3–4):147–151

22. Ghasemi A, Hossienpour A, Morisako A, Saatchi A, Salehi M (2006) Electromagnetic properties and microwave absorbing characteristics of doped barium hexaferrite. J Magn Magn Mater 302(2):429–435
23. Narang SB, Kaur P, Bahel S, Singh C (2016) Microwave characterization of Co–Ti substituted barium hexagonal ferrites in X-band. J Magn Magn Mater 405:17–21
24. Kaur H, Singh C, Marwaha A, Narang SB, Jotania R, Mishra SR, Bal Y, Raju KCJ, Singh D, Ghimire M, Sombra ASB, Dhruv P (2018) Investigation of structural, elucidation of microwave absorption mechanisms in Co-Ga substituted Ba-Sr hexaferrites in X-band. J Mater Sci Mater Electron 29:14995–15005